Electronic Supplementary Material (ESI) for Dalton Transactions.

Supplementary Information Available

Highly-Fluorescent BODIPY-functionalised Metallacages as Drug Delivery Systems: Synthesis, Characterisation and Cellular Accumulation Studies

Brech Aikman,[a,†] Riccardo Bonsignore,[a,b,†] Ben Woods,[c] Daniel Doellerer,[d] Riccardo Scotti,[a] Claudia Schmidt,[a] Alexandra A. Heidecker,[e] Alexander Pöthig,[e] Edward J. Sayers,[f] Arwyn T. Jones[f,*] and Angela Casini[a,g,*]

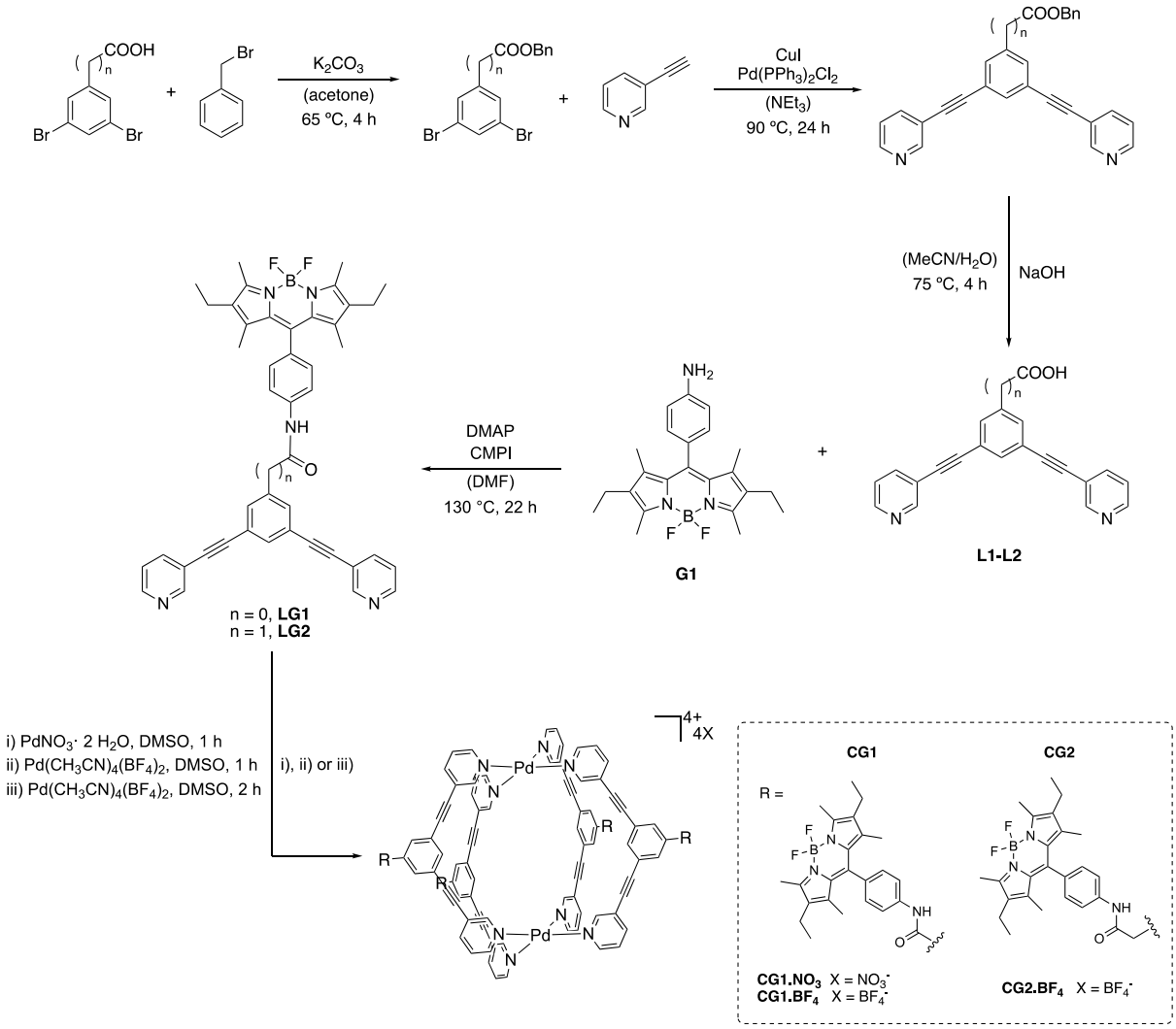

Scheme S1. Overall synthetic pathways leading to cages **CG1.X and CG2.BF_4**.

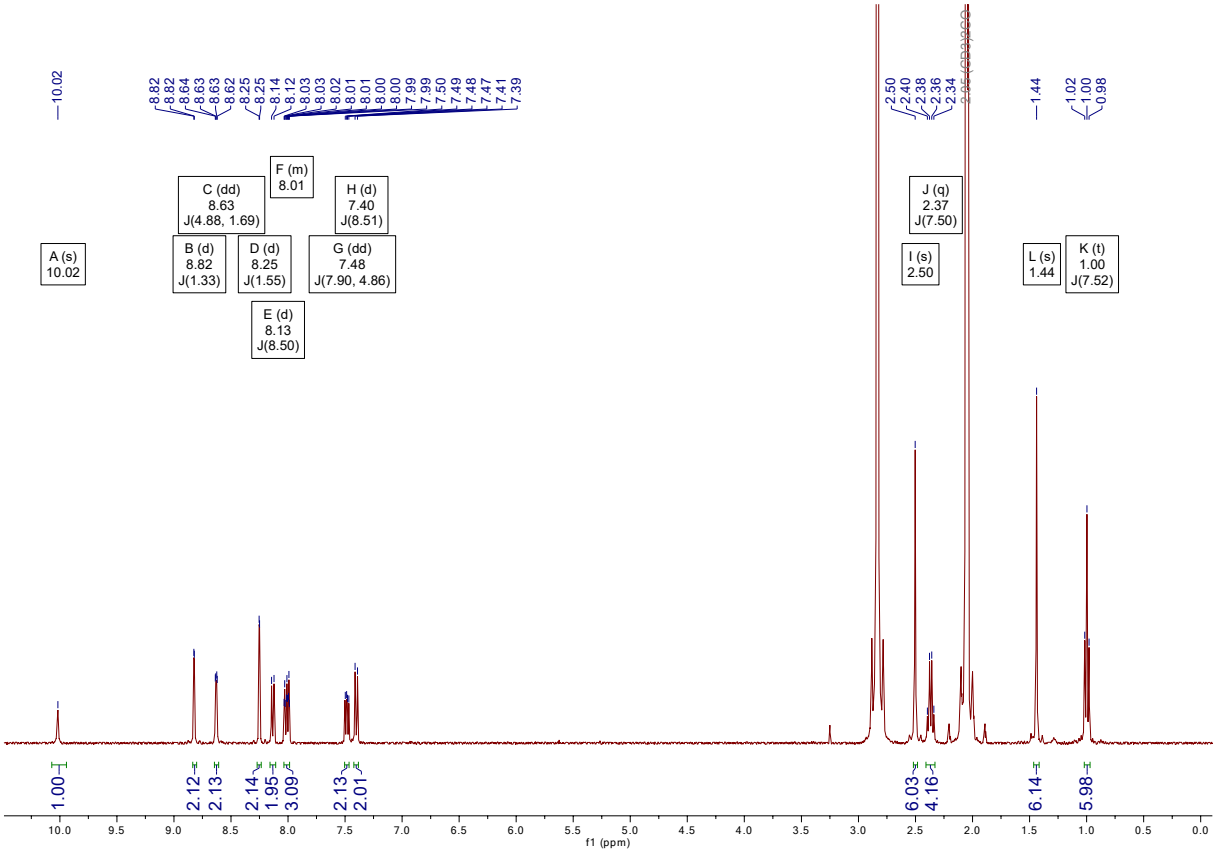

Figure S1. ^{1}H NMR (400 MHz, acetone-d_6) spectrum of **LG1**.

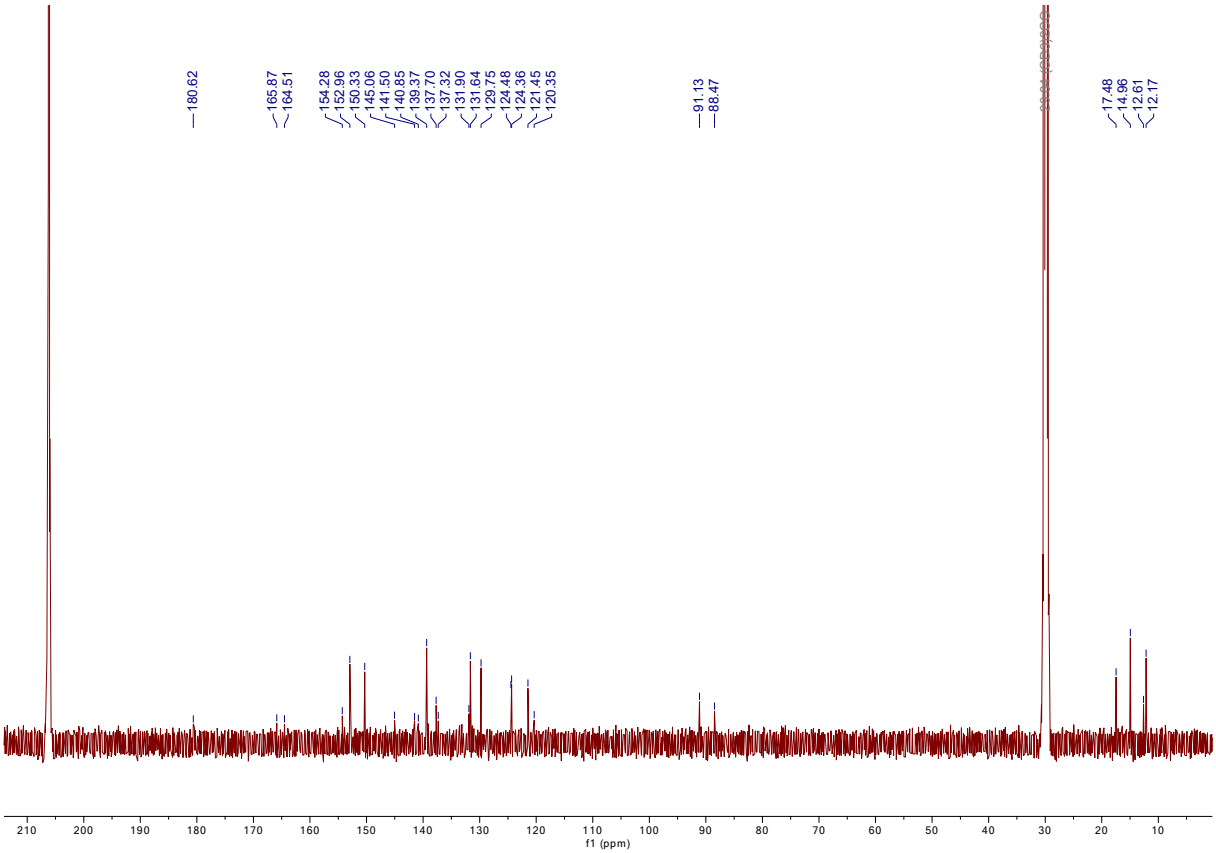

Figure S2. ^{13}C NMR (126 MHz, acetone-d_6) spectrum of **LG1**.

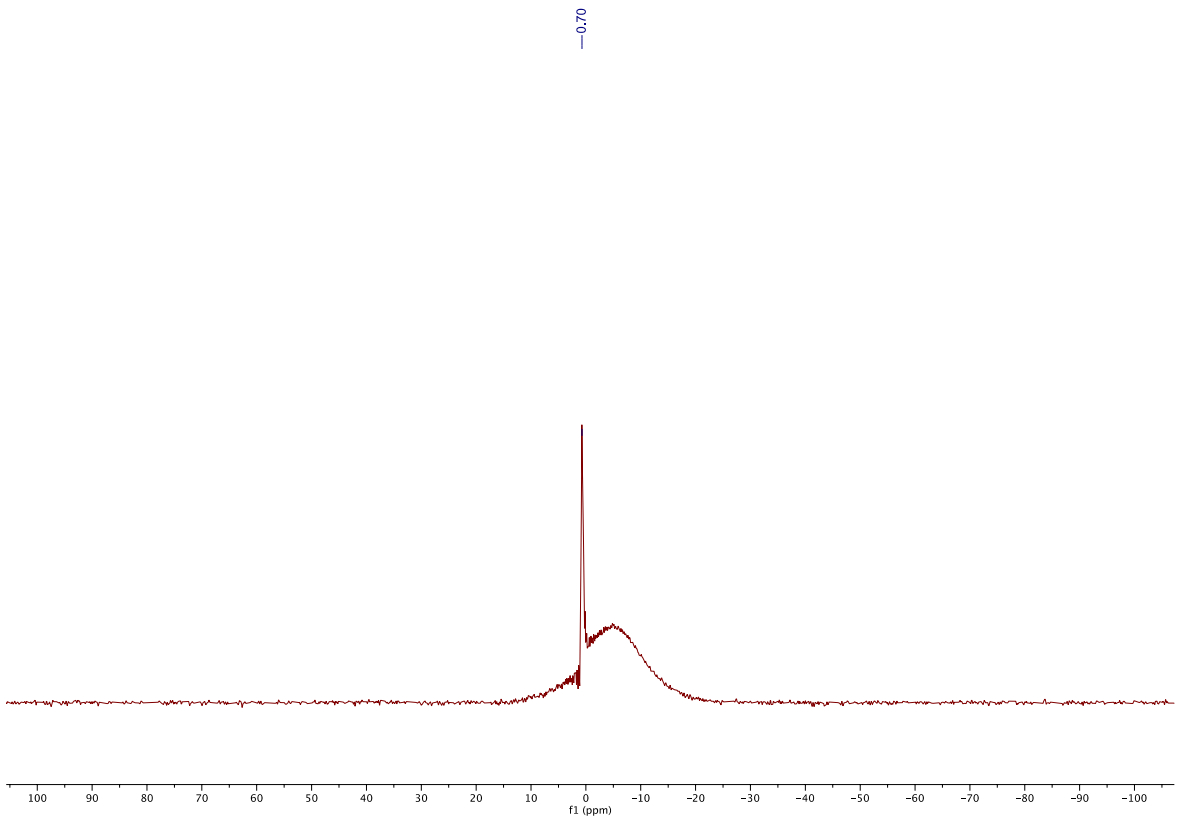

Figure S3. ^{11}B NMR (160 MHz, acetone-d_6) spectrum of **LG1**.

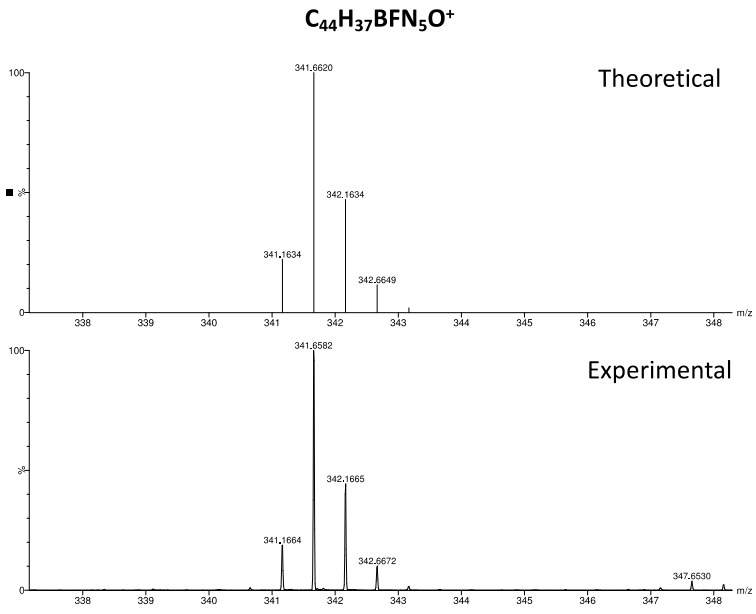

Figure S4. Theoretical and experimental HR-ESI-MS of **LG1** in MeOH.

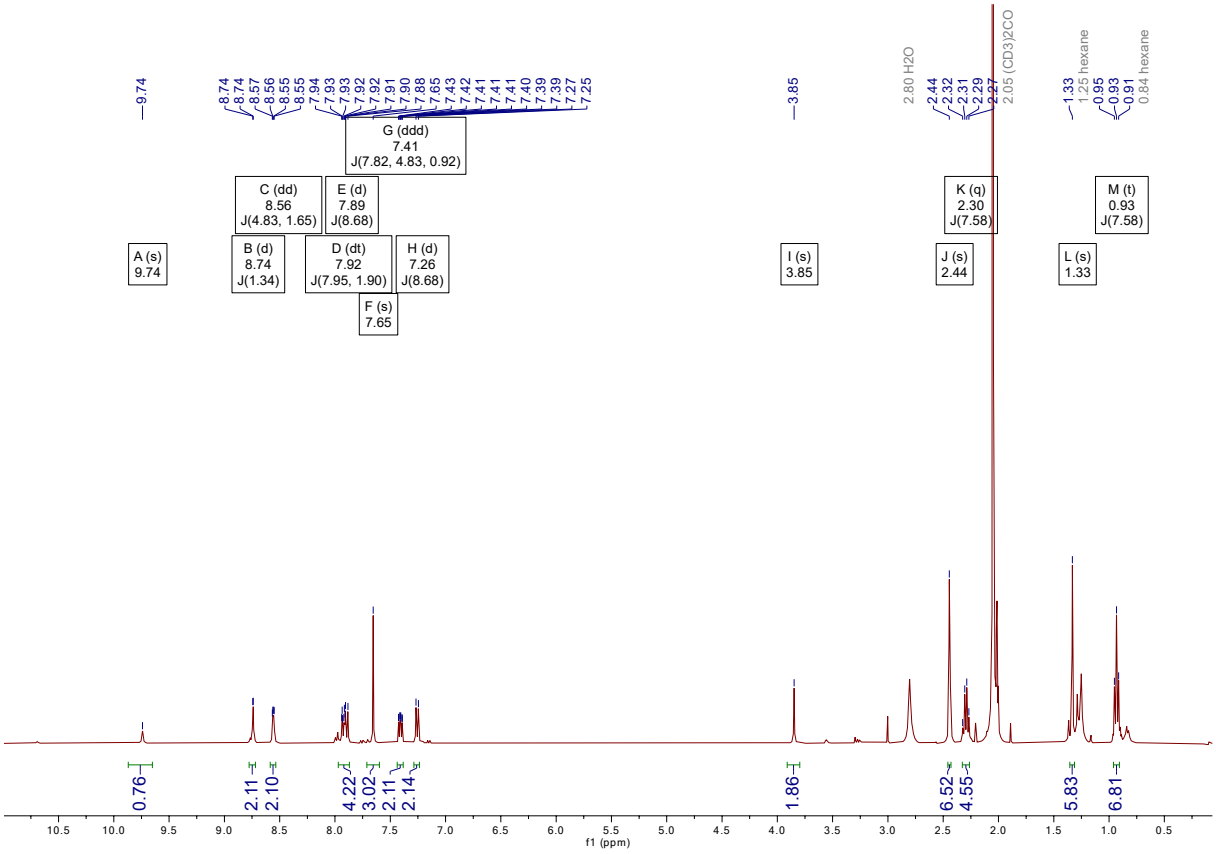

Figure S5. ^{1}H NMR (400 MHz, acetone-d_6) spectrum of **LG2**.

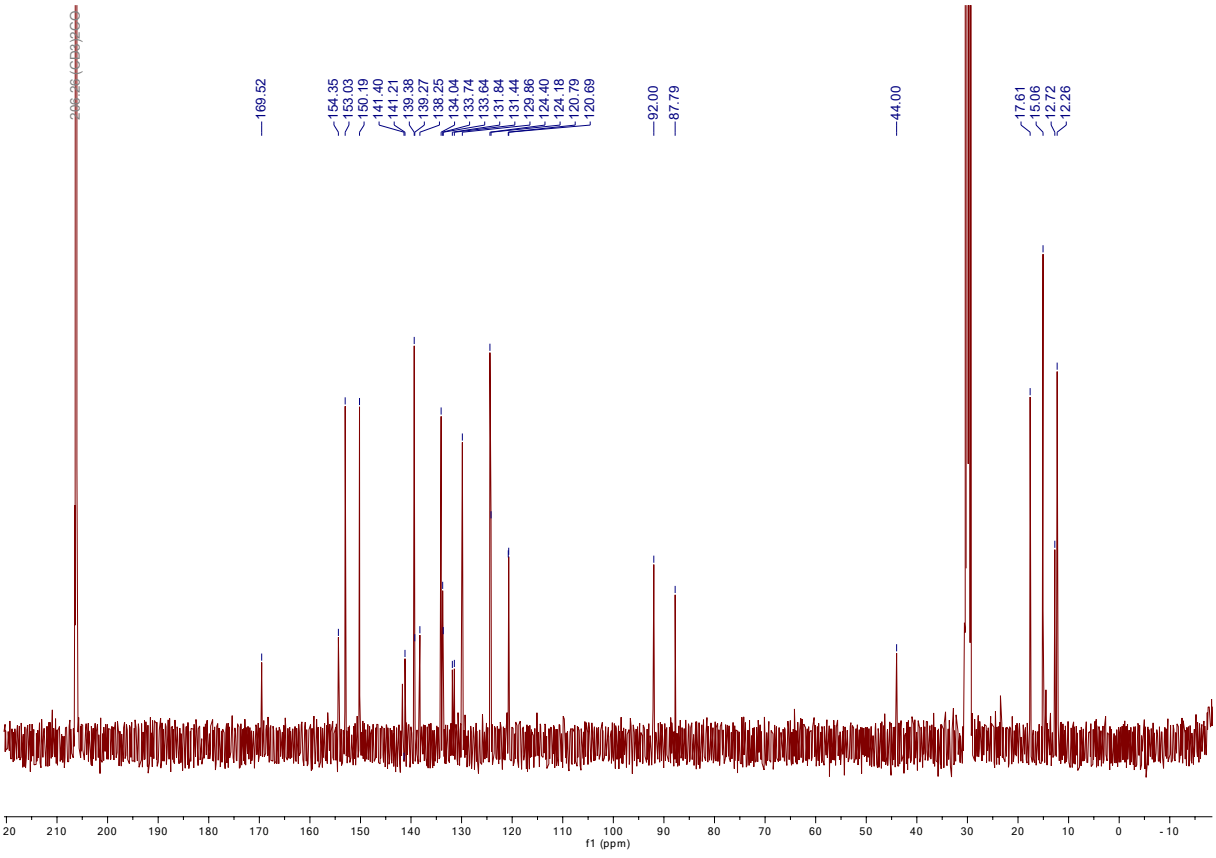

Figure S6. ^{13}C NMR (101 MHz, acetone-d_6) spectrum of **LG2**.

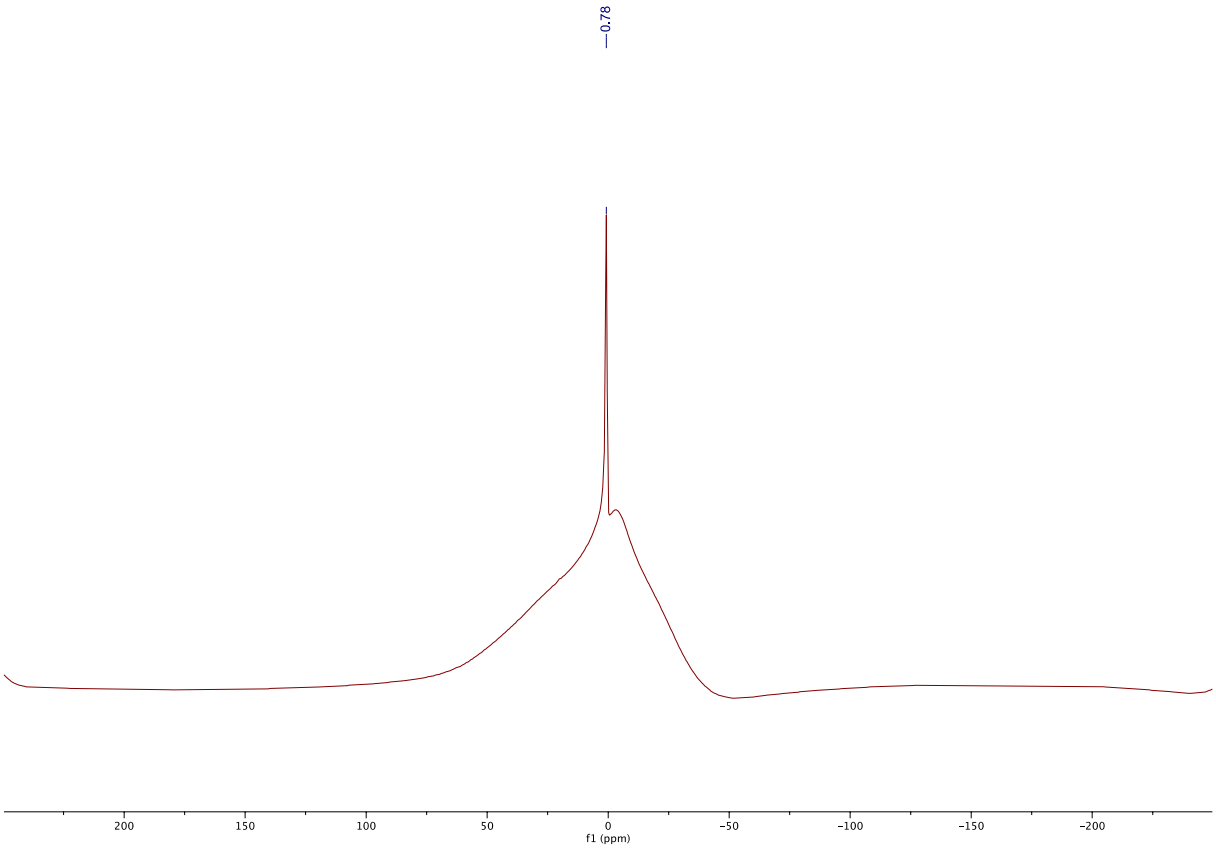

Figure S7. ^{11}B NMR (128 MHz, acetone-d_6) spectrum of **LG2**.

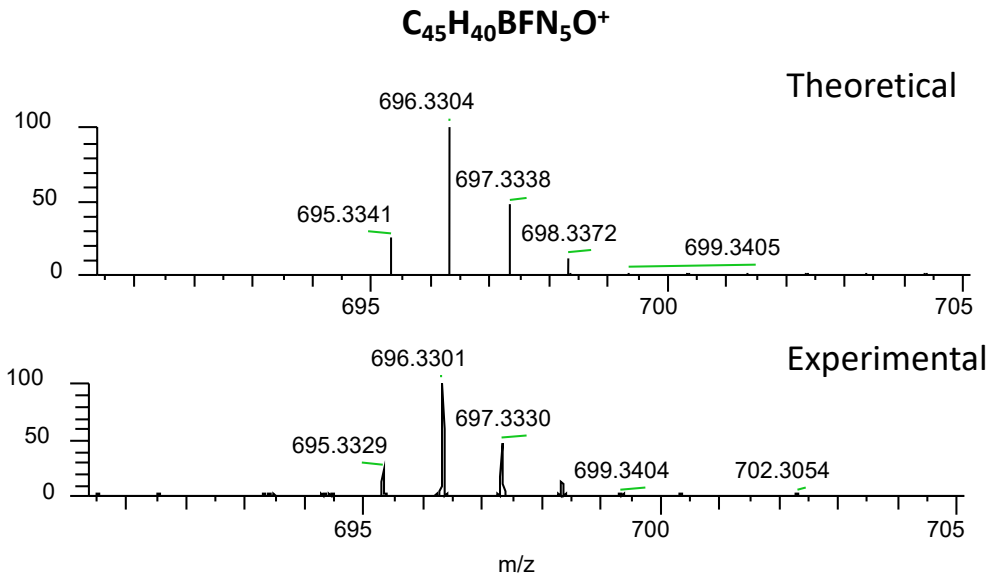

Figure S8. Theoretical and experimental HR-ESI-MS spectrum of **LG2** in DCM:DMF (1:1).

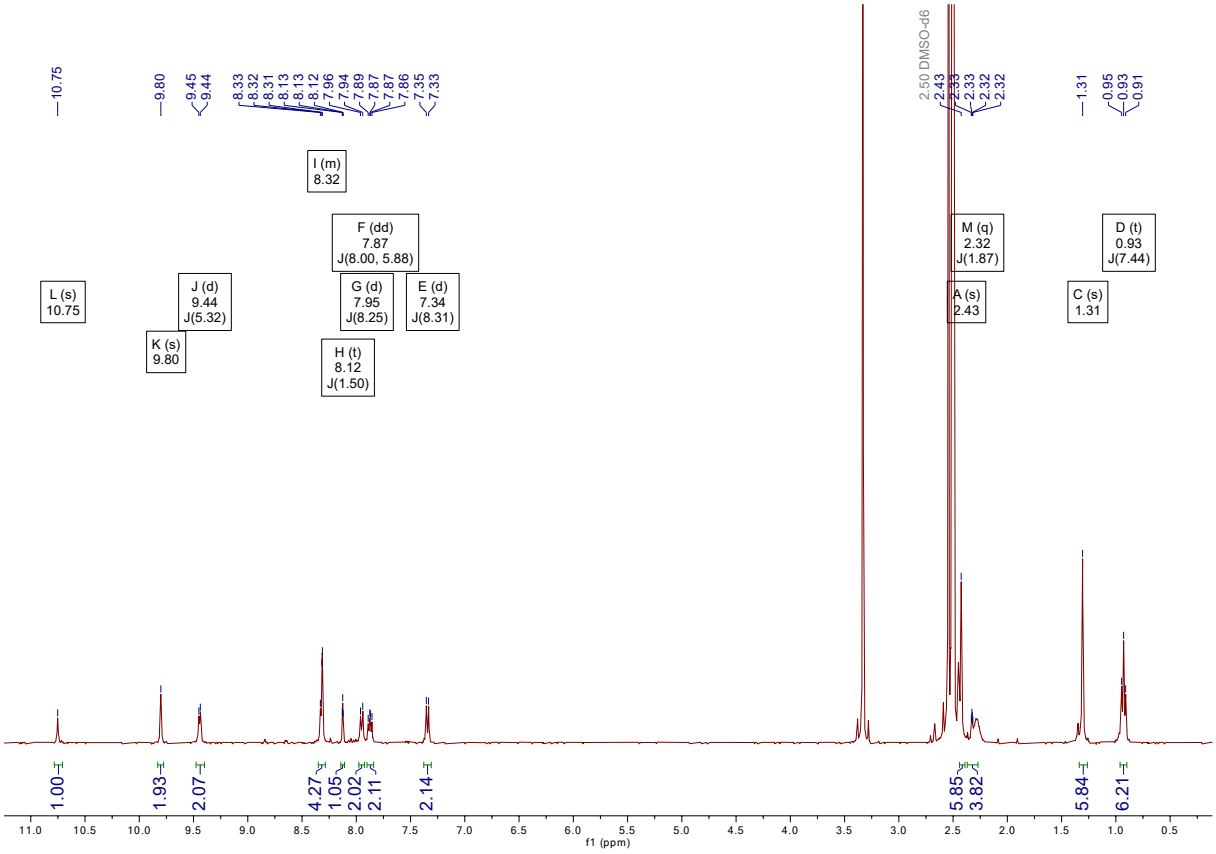

Figure S9. ^{1}H NMR (500 MHz, DMSO-d_6) spectrum of **CG1.X**.

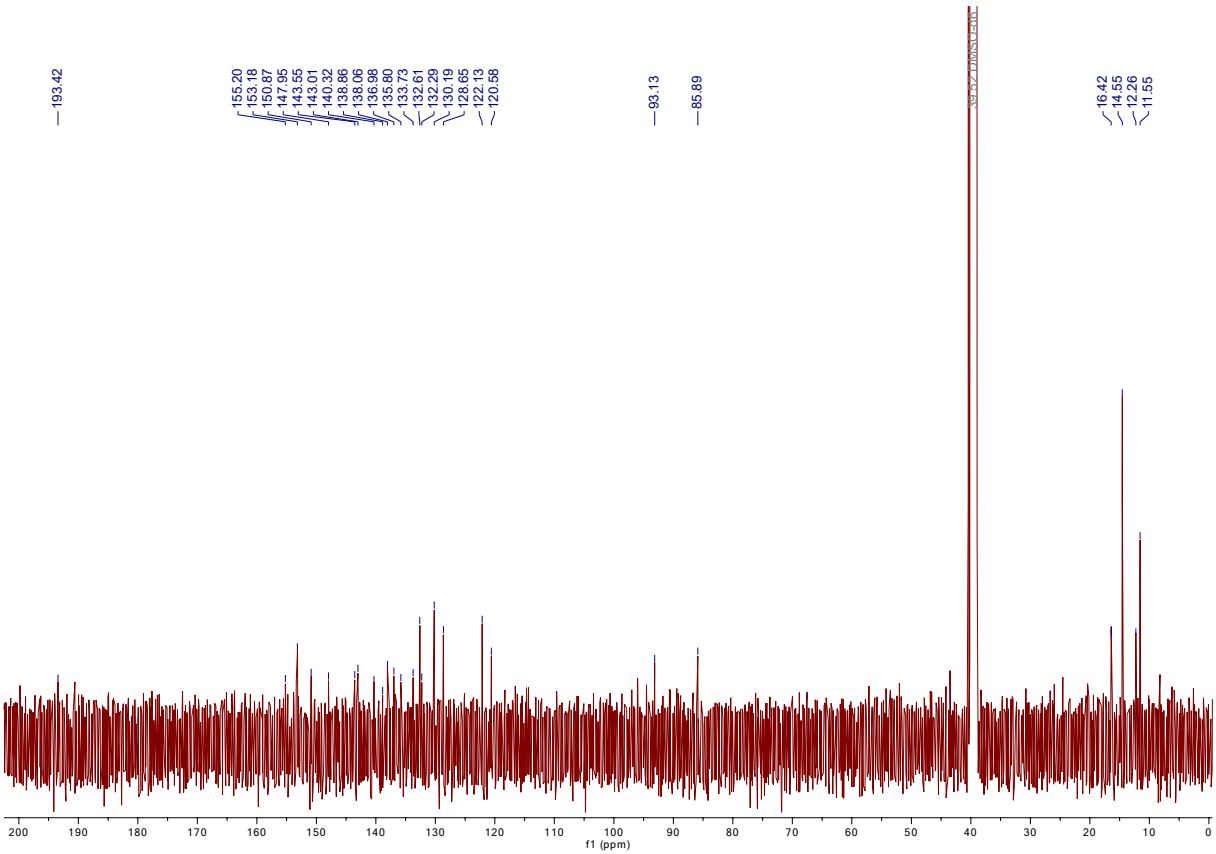

Figure S10. ^{13}C NMR (126 MHz, DMSO-d_6) spectrum of **CG1.X**.

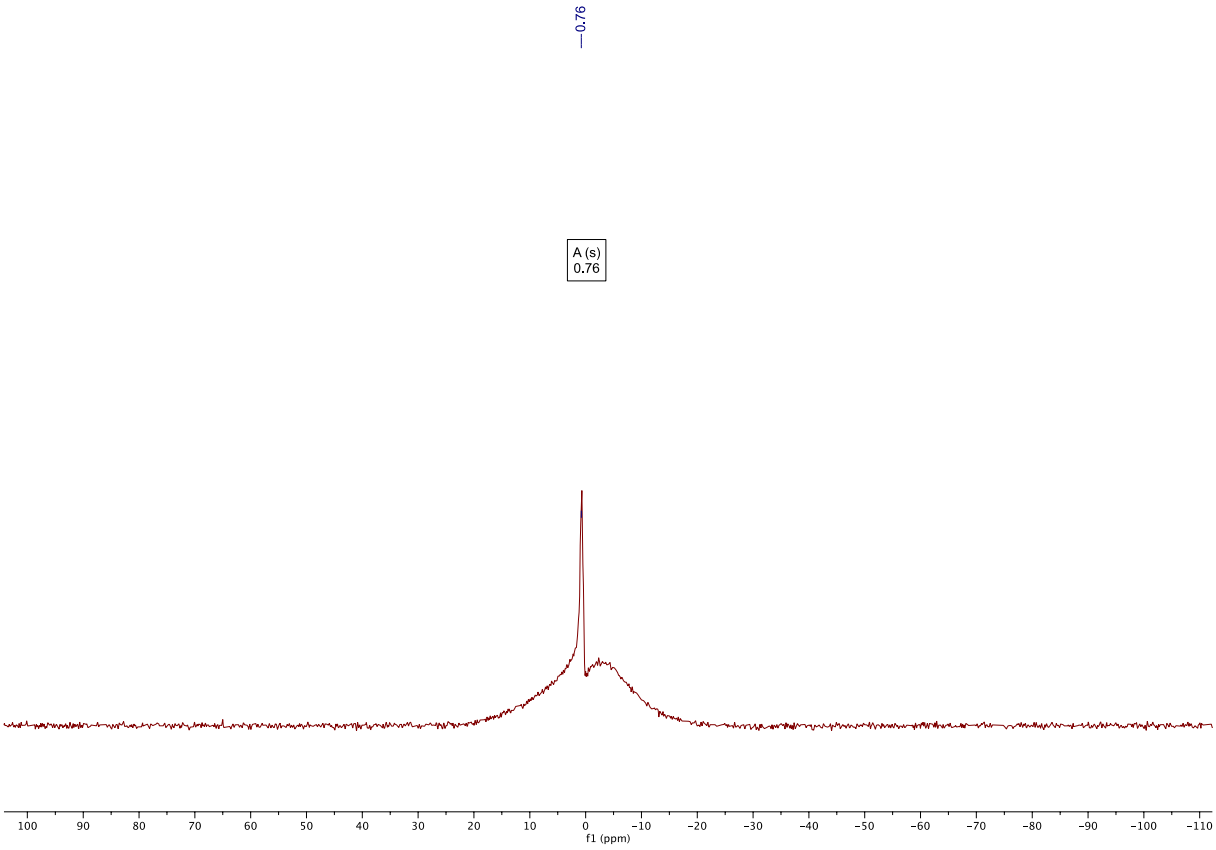

Figure S11. ^{11}B NMR (128 MHz, DMSO-d_6) spectrum of **CG1.X**.

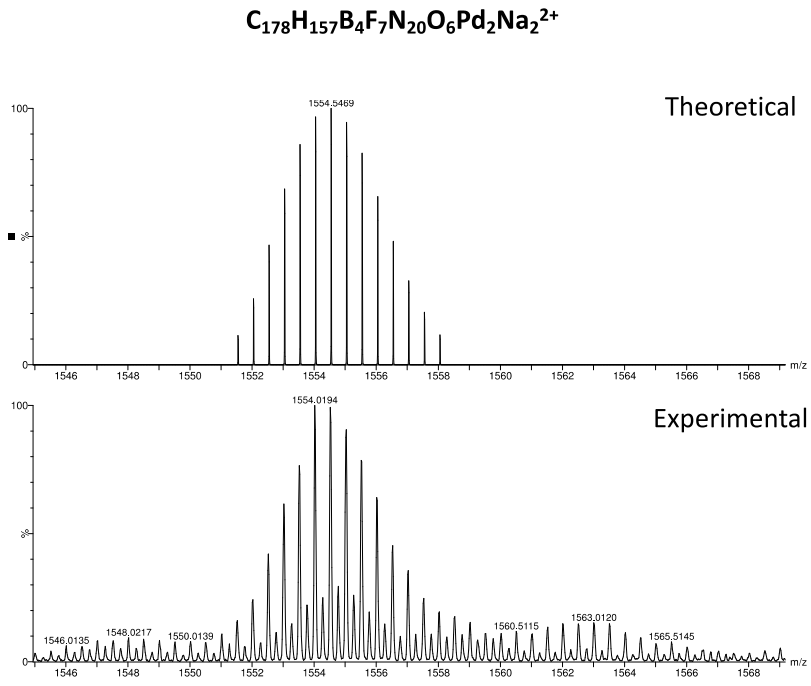

Figure S12. Theoretical and experimental HR-ESI-MS spectrum of **CG1.X** in MeOH.

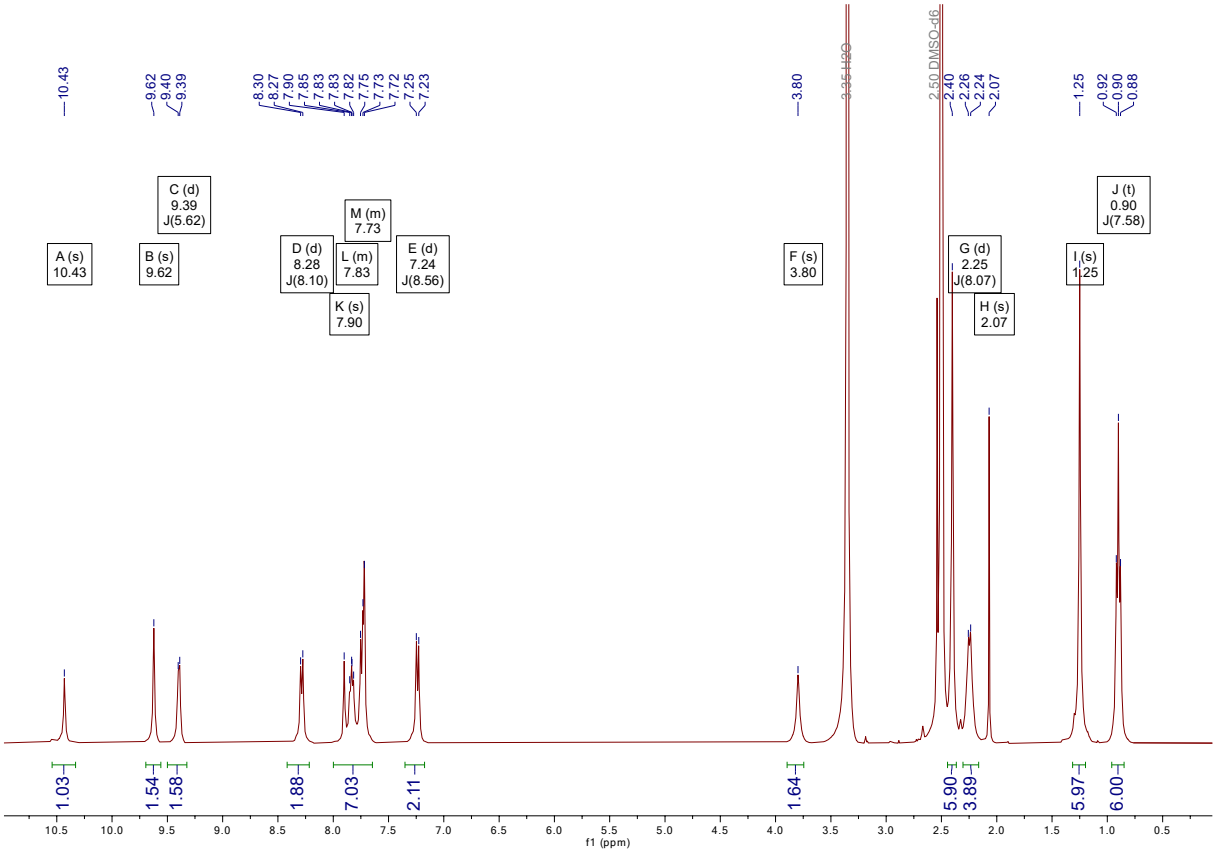

Figure S13. ^{1}H NMR (400 MHz, DMSO-d_6) spectrum of **CG2.BF$_4$**.

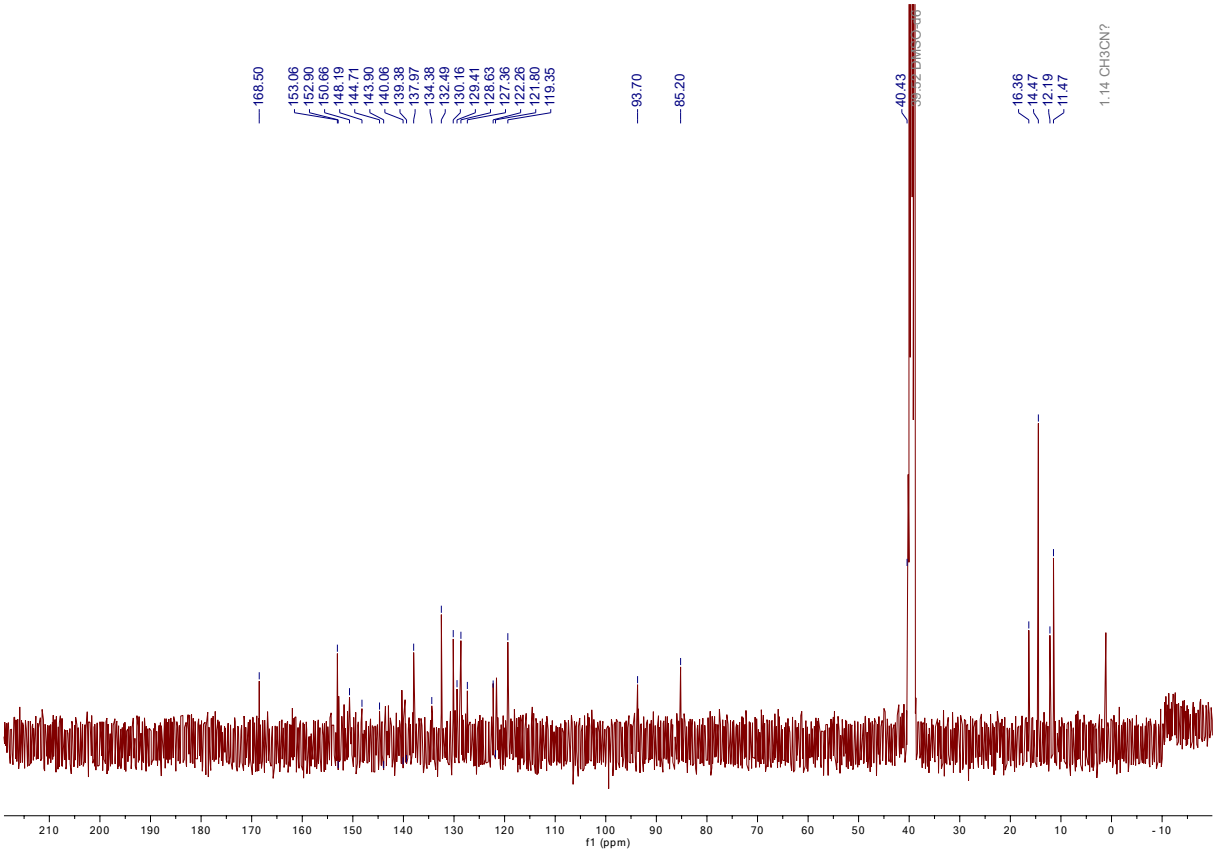

Figure S14. ^{13}C NMR (101 MHz, DMSO-d_6) spectrum of **CG2.BF$_4$**.

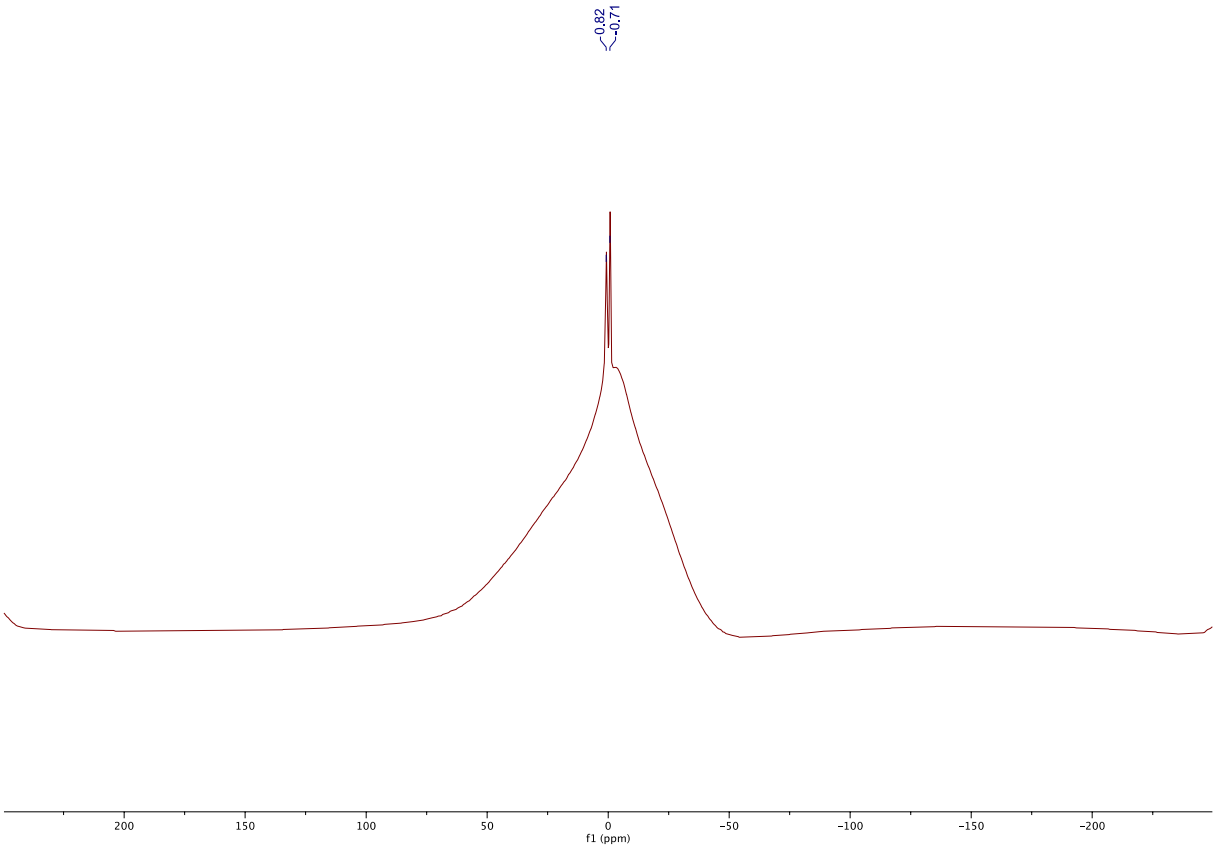

Figure S15. ^{11}B NMR (128 MHz, ACN-d_3) spectrum of **CG2.BF$_4$**.

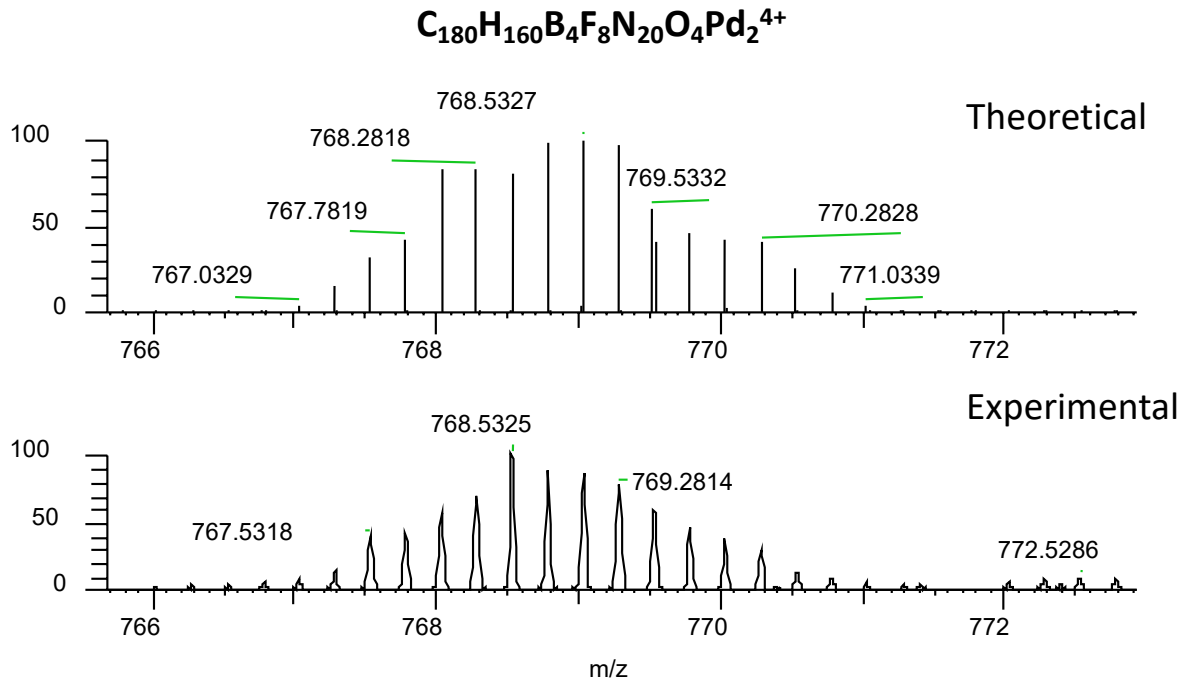

Figure S16. Theoretical and experimental HR-ESI-MS spectrum of **CG2.BF$_4$** in DCM:DMF (1:1).

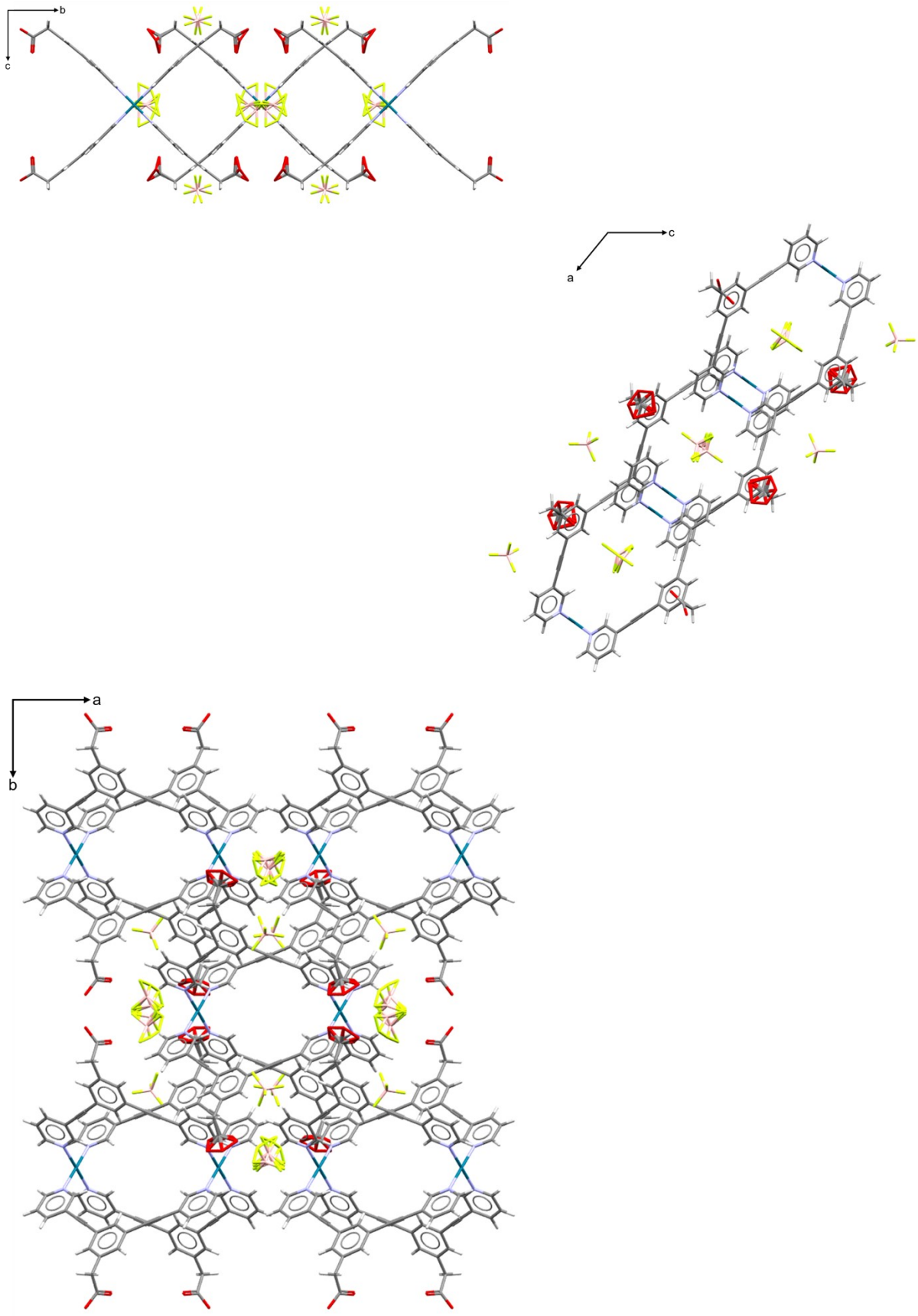

Figure S17 - Crystal Packing of $[Pd_2\mathbf{L2}_4]^{4+}$ along a- (top), b- (middle) and c-axis (bottom). Atoms are displayed as capped sticks.

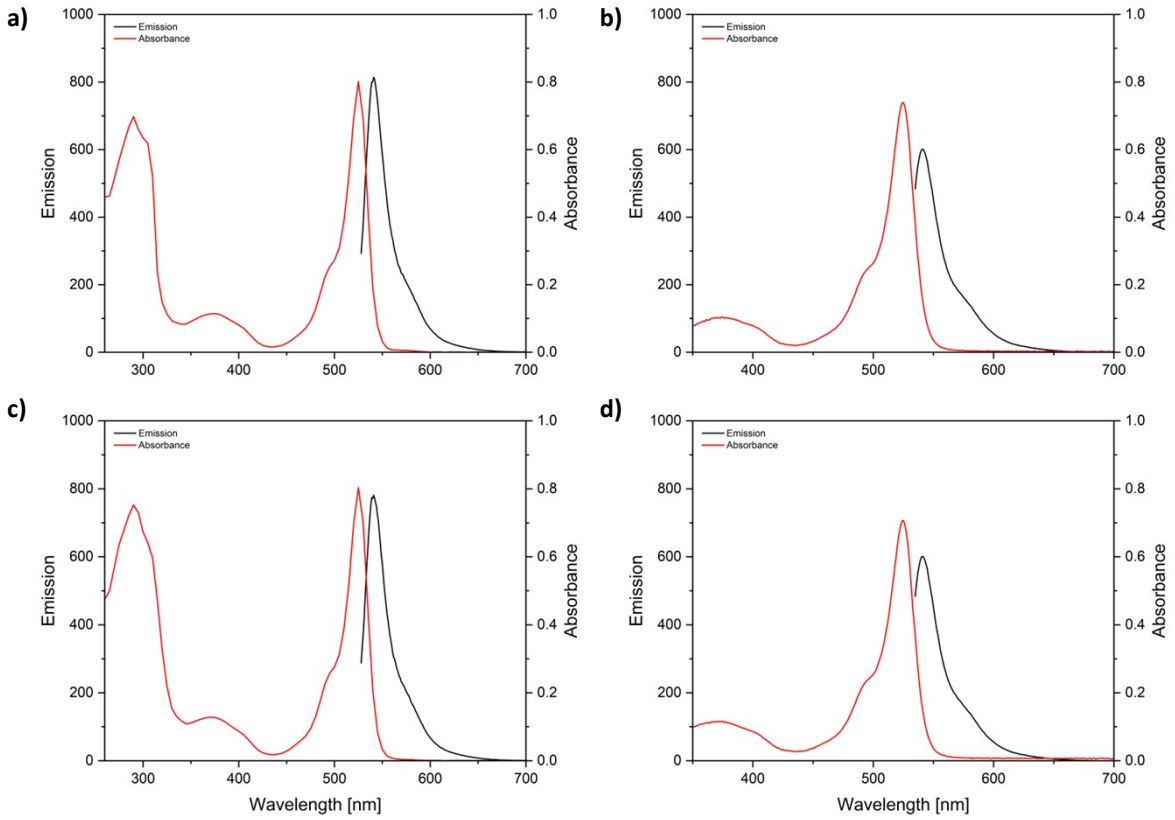

Figure S18. Absorbance (red) and emission (black) spectra in DMSO of **LG1** (a, 10.0 μM), **LG2** (b, 13.8 μM), **CG1.NO$_3$** (c, 3.5 μM) and **CG2.BF$_4$** (d, 2.5 μM).

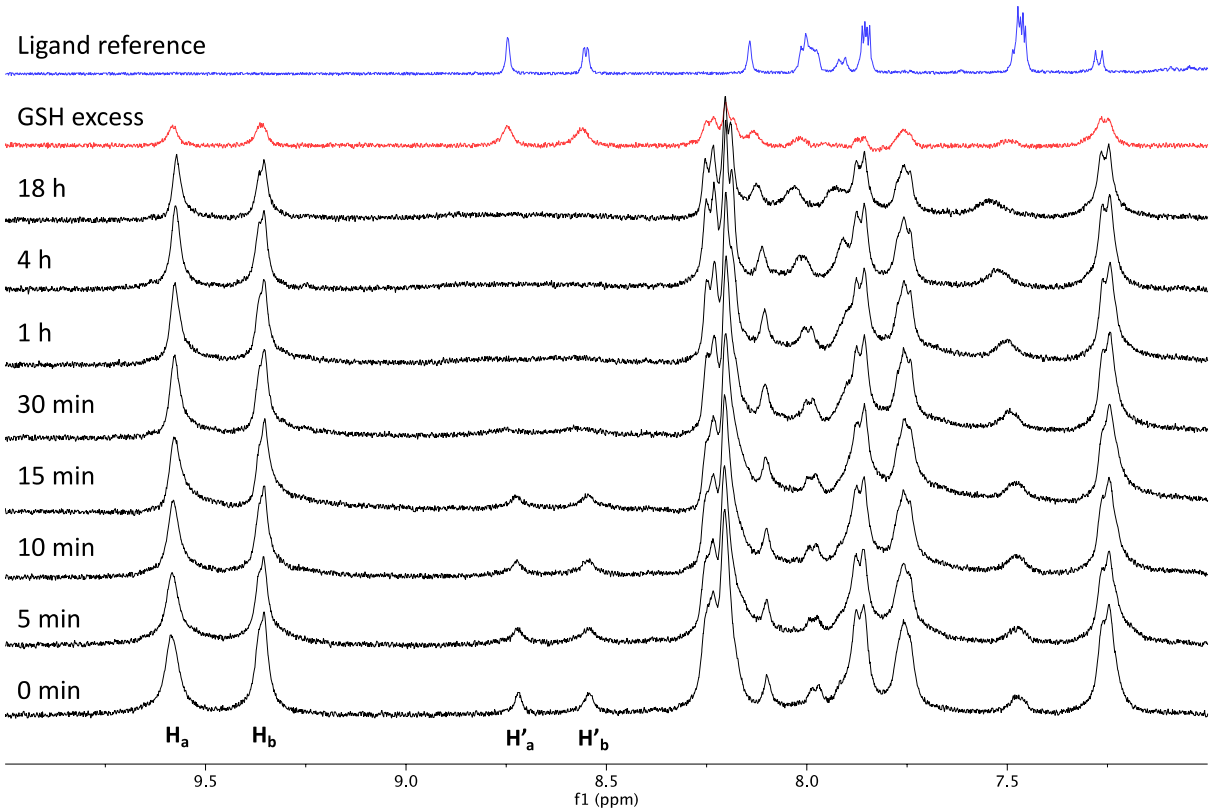

Figure S19. - Stacked ^{1}H NMR spectra of ligand **LG1** (blue spectrum) and of the corresponding metallacage **CG1.BF$_4$** (second trace from top) after addition of 1 equiv. glutathione (GSH, 2 mM) in 9:1 ratio of DMSO-d_6: D_2O, followed over time. A further addition of excess GSH (4 mM) was performed after 18 h (red spectrum).

A)

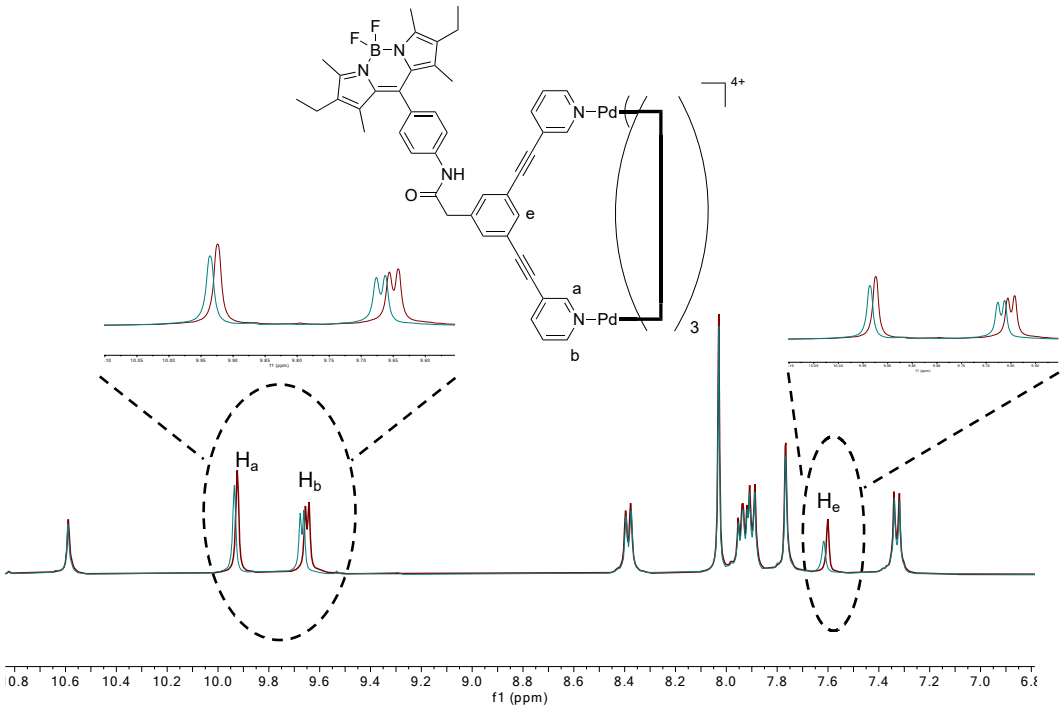

B)

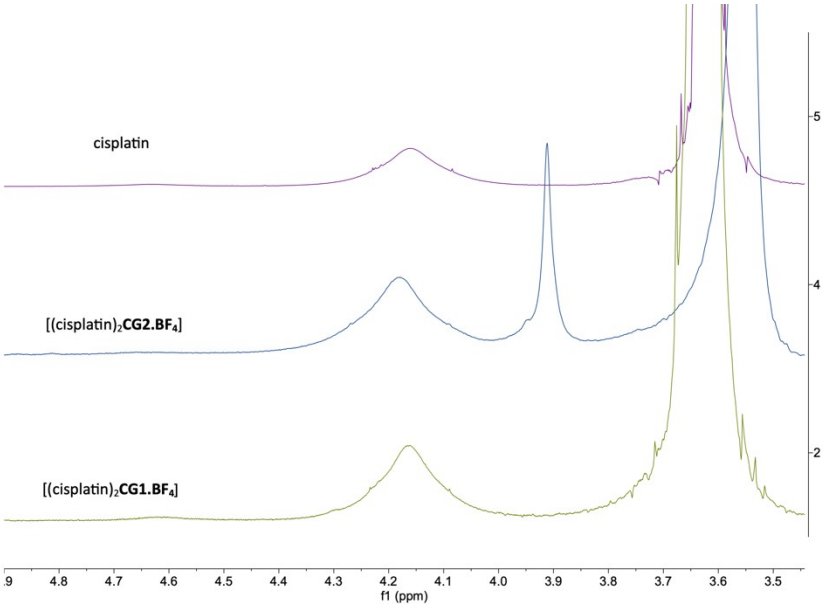

Figure S20 – Cisplatin encapsulation in a metallacage. **A**) Stacked ^{1}H NMR spectra of cage **CG2.BF$_4$** in DMF-$_{d7}$ (red trace) alone and after the addition of 2 equiv. of cisplatin (green trace) to form the [(cisplatin)$_2$⊂**CG2.BF$_4$**] host-guest complex. Zoomed region between 10.8-6.8 ppm. **B**) Stacked ^{1}H NMR spectra of [(cisplatin)$_2$⊂**CG1.BF$_4$**] and [(cisplatin)$_2$⊂**CG2.BF$_4$**] host-guest complexes in DMF-$_{d7}$ in comparison to cisplatin. Zoomed region between 4.9 – 3.5 ppm.

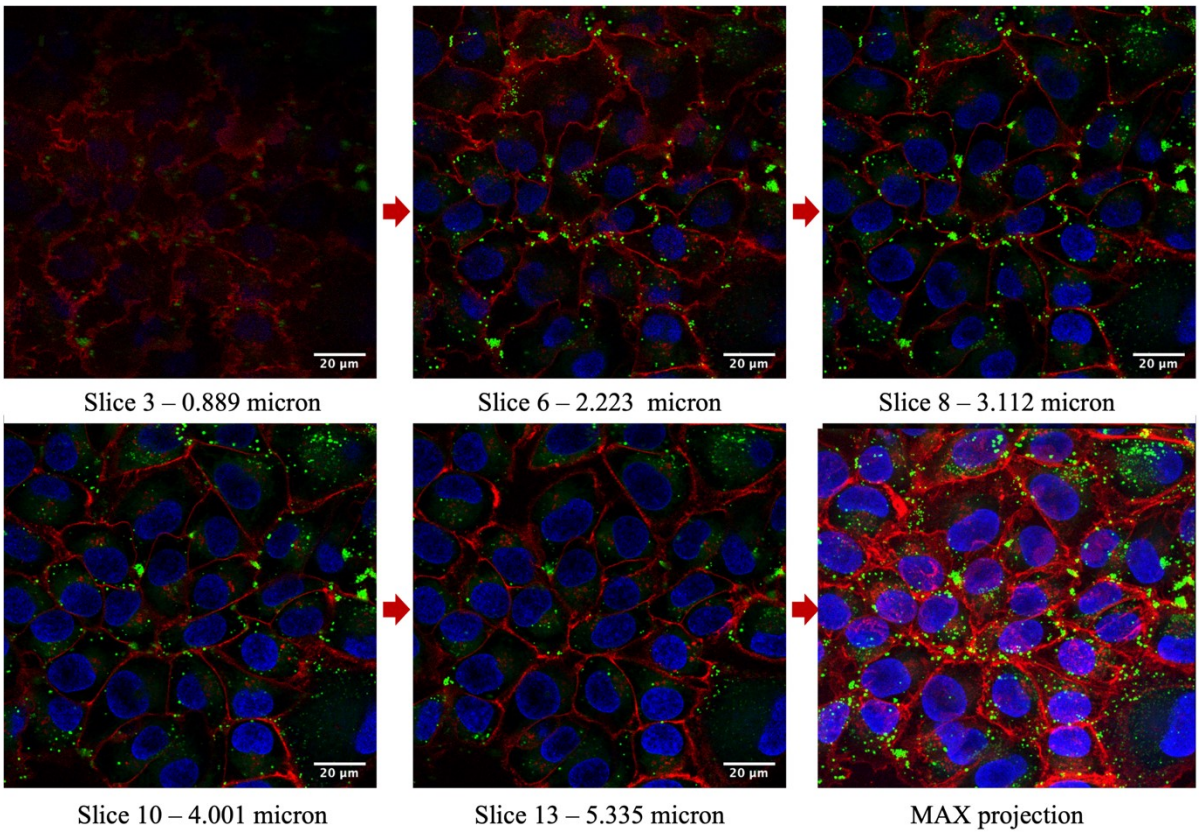

Figure S21 - Selection of single z-stack CLSM images of A375 cells treated with **CG1.NO$_3$** (green) for 2 h, with generated MAX projection. Plasma membrane is marked with CellMask™ Deep Red, counterstaining performed with nuclear dye Hoechst (blue). Images enhanced after acquisition. Scale bar 20 µm.

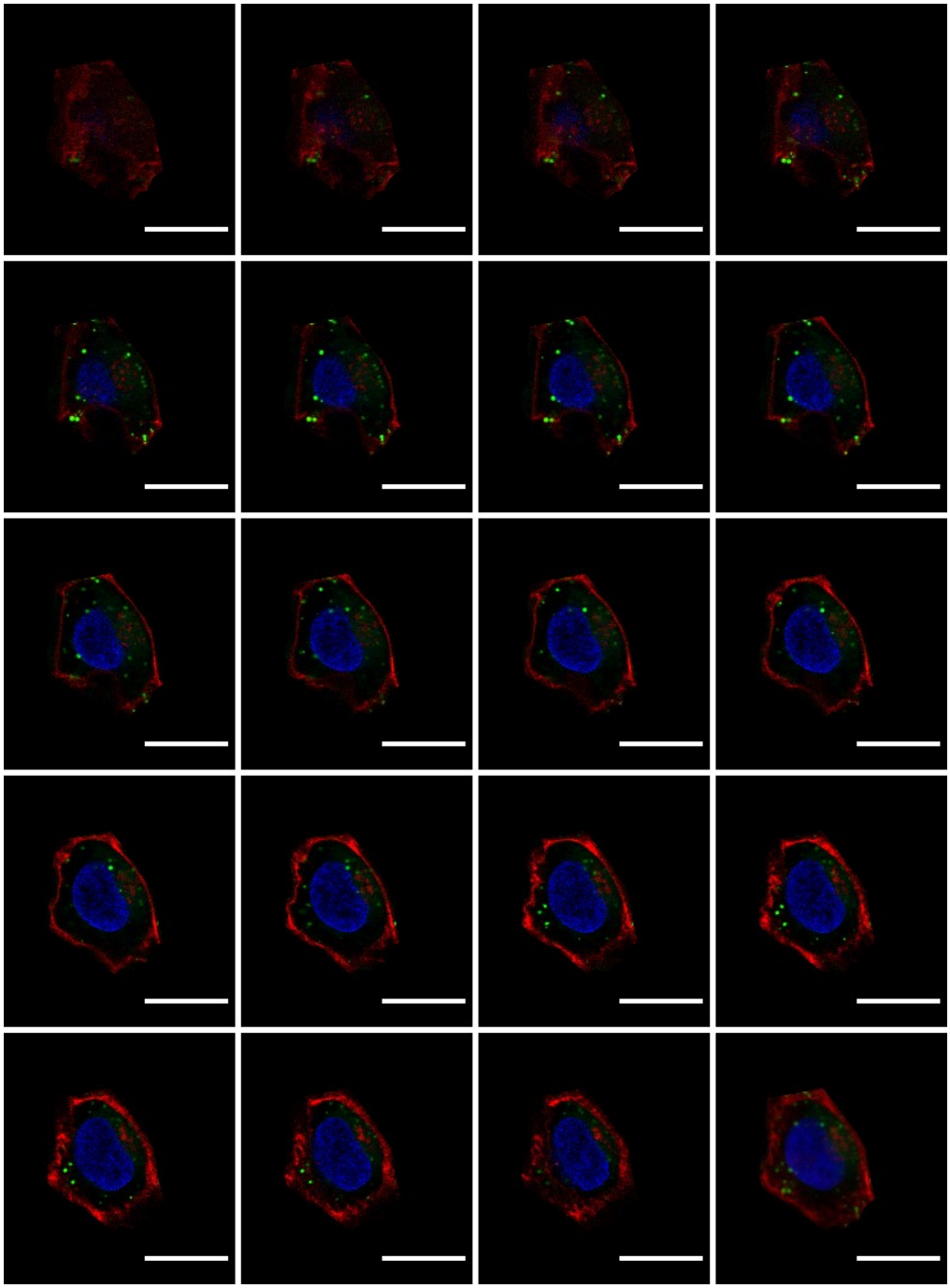

Figure S22 - Complete z-stack CLSM images of single A375 cell (selected from Figure S21) treated with 5 μM **CG1.NO$_3$** for 2 h. Scale bar represents 20 μm.

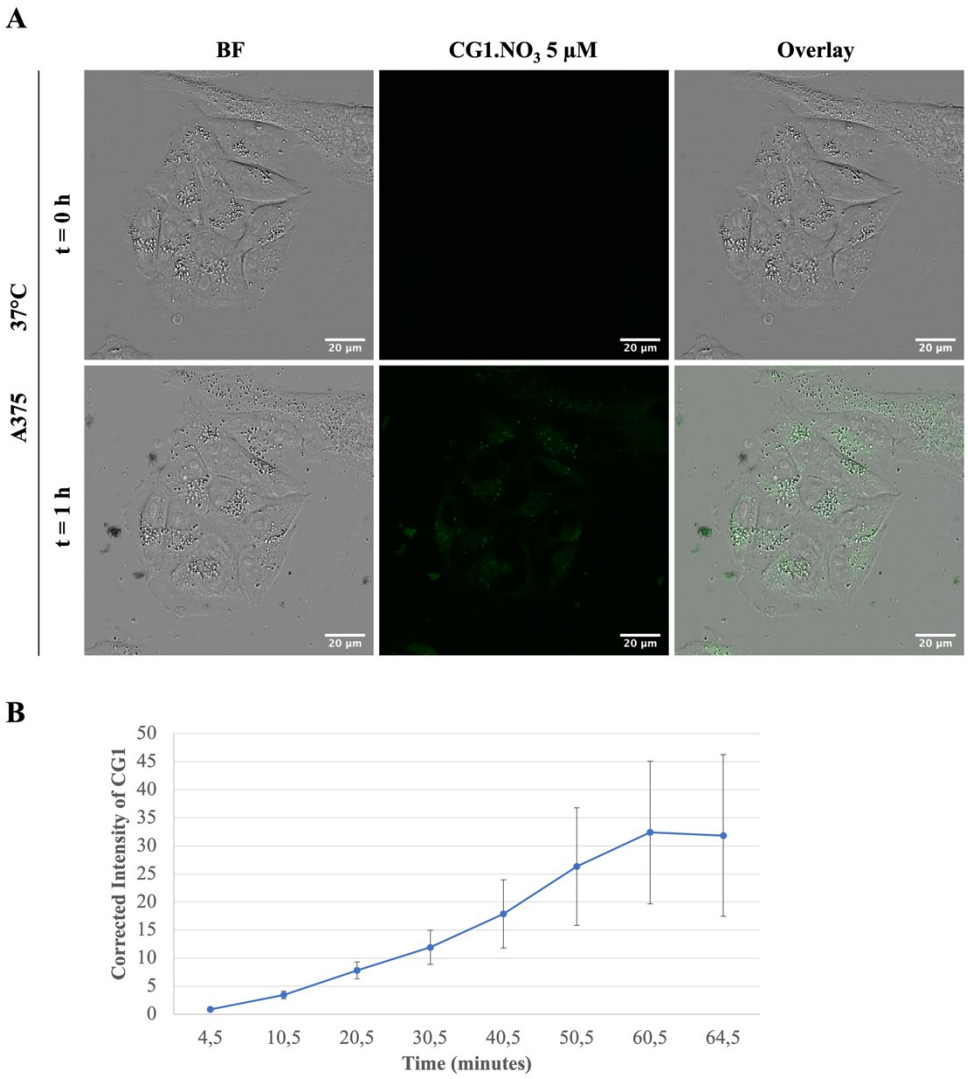

Figure S23 - **A)** CLSM images of human A375 cells incubated with 5 µM of **CG1.NO$_3$** cage at t ≅ 0 h and t ≅ 1 h. Scale bar is 20 µm. BF = bright field. **B)** Graph detailing fluorescent intensity after **CG1.NO$_3$** administration with standard deviation, calculated for mean of five representative intracellular regions of interest (ROI) and corrected for corresponding background intensity over time. The initial time lag of ca. 4.5 min was from acclimatization of cells before acquisition. The full time-course is shown in Supplementary Movie 1.

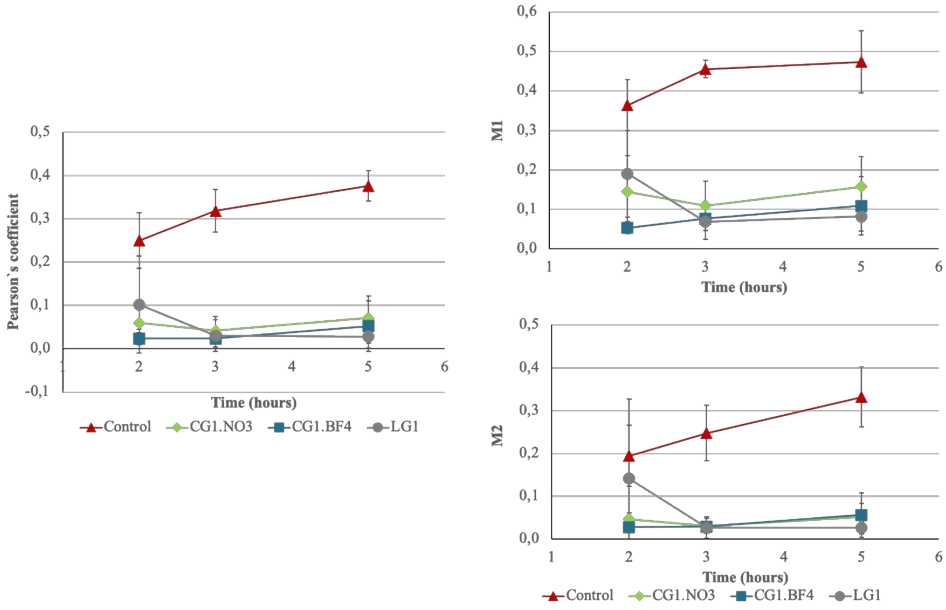

Figure S24 - Pearson`s correlation coefficient and Manders M1 & M2 with corresponding standard deviation describing fluorescent intensity overlap between ligand/cage complexes/control and lysosomes labelled with Dex-647. M1 is the summed intensity of pixels from the compound/control that have intensity above zero in the red Dex-647 image, and M2 vice versa.

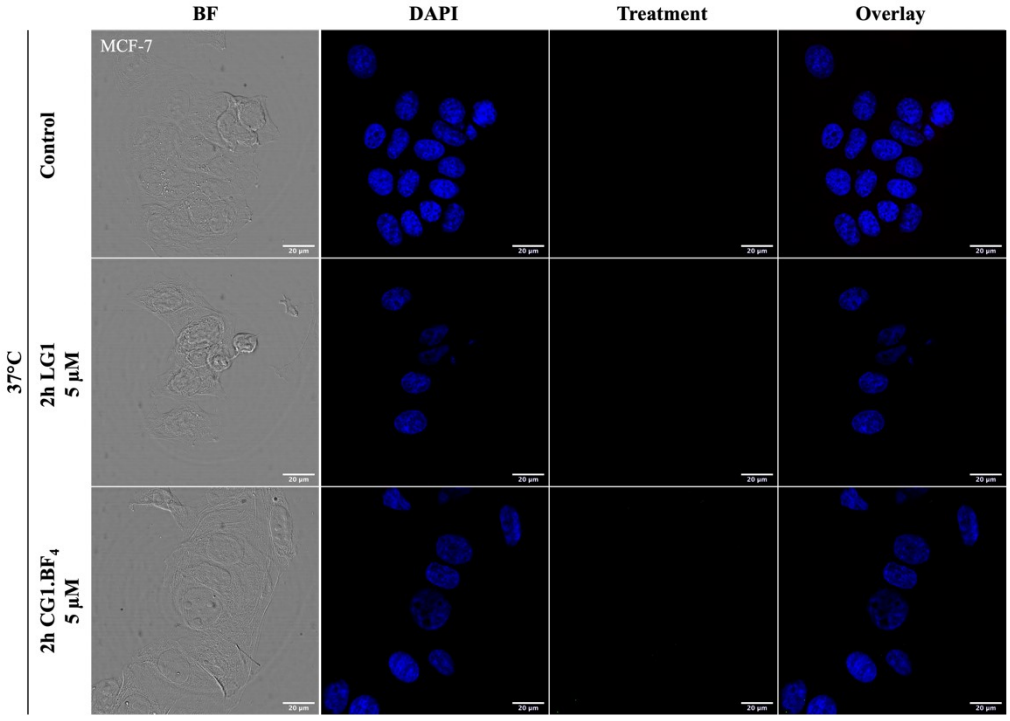

Figure S25 – Fluorescence widefield microscopy images of fixed human MCF7 cells incubated without or with (5 µM) **CG1.BF$_3$** or **LG1** for 2 h at 37 °C. Counterstaining of nucleus with DAPI. Scale bar 20 µm.

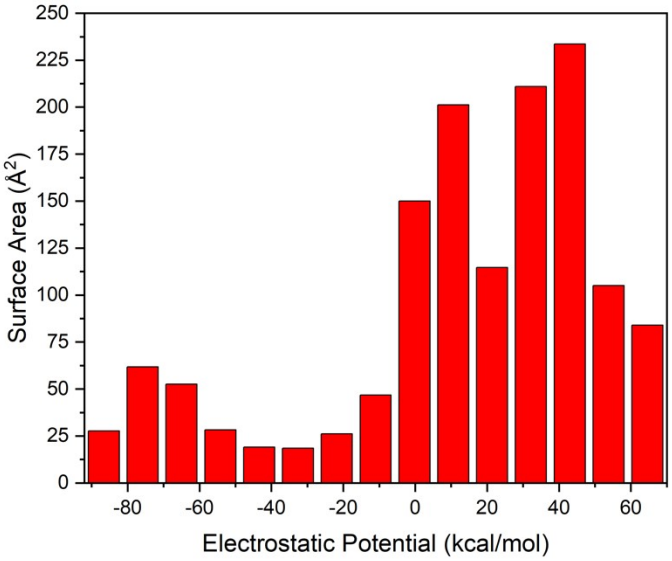

Figure S26 - The surface area is represented in the ESP range on the vdW surface of [Pd**L2**$_4$]$^{4+}$

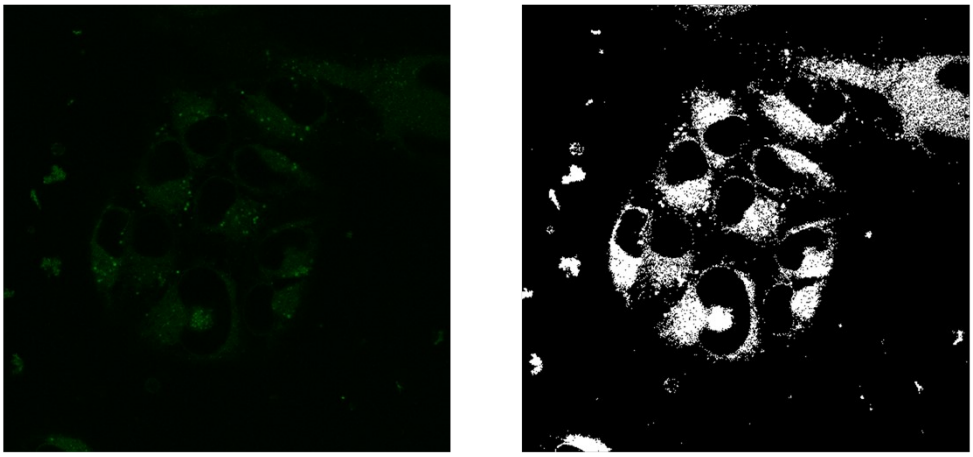

Image before processing	Otsu treshold applied

Figure S27 - Example illustrating use of threshold. Image on the left shows A375 cells at t = 64.5 min. Image on the right is the same shot, converted so that white represent pixel intensity above threshold set by “Otsu” and black below threshold.

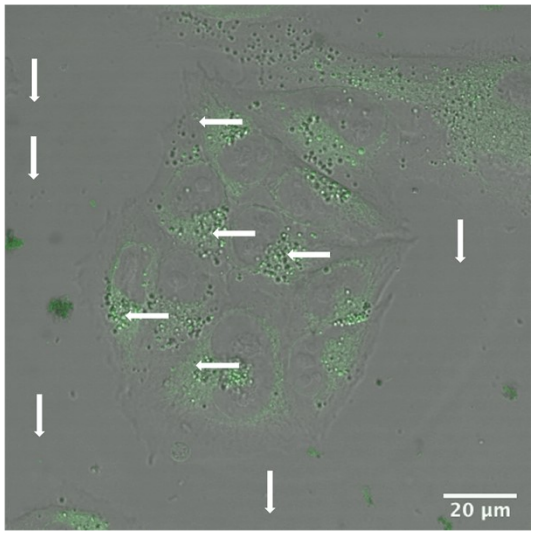

Figure S28- Example illustrating use of regions of interest (ROI) indicated by arrows, with 5 background and 5 intracellular selections.

Crystallographic data of $[Pd_2\mathbf{L2}_3\mathbf{L2^*}]^{3+}(BF_4)_3$ (CCDC 2143205).

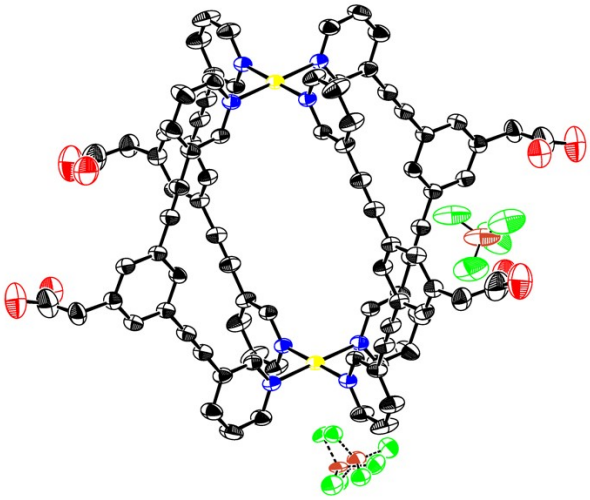

Figure A: ORTEP Plot of the crystal structure of $[Pd_2\mathbf{L2}_4]^{4+}$*. ADPs are given at the 50% probability level; hydrogen atoms are omitted for clarity.*

Table S1: Table of crystal data, data collection and structure refinement of $[Pd_2\mathbf{L2}_4]^{4+}$.

Identification code	SchCl4	
Chemical formula	$C_{44}H_{26}B_{1.50}F_6N_4O_4Pd$	
Formula weight	911.30	
Temperature	123(2) K	
Wavelength	0.71073 Å	
Crystal size	0.050 x 0.214 x 0.277 mm	
Crystal system	monoclinic	
Space group	C 1 2/m 1	
Unit cell dimensions	a = 20.261(2) Å	α = 90°
	b = 21.251(2) Å	β = 125.712(2)°
	c = 17.3423(17) Å	γ = 90°
Volume	6062.9(10) $Å^3$	
Z	4	
Density (calculated)	0.998 g/cm^3	
Absorption coefficient	0.357 mm^{-1}	
F(000)	1830	

Diffractometer	Bruker D8 Venture

Radiation source	TXS rotating anode, Mo	
Theta range for data collection	2.40 to 25.68°	
Index ranges	-24<=h<=24, -25<=k<=25, -21<=l<=21	
Reflections collected	120044	
Independent reflections	5923 [R(int) = 0.0468]	
Max. and min. transmission	0.9820 and 0.9080	
Structure solution technique	direct methods	
Structure solution program	SHELXT 2014/5 (Sheldrick, 2014)	
Refinement method	Full-matrix least-squares on F^2	
Refinement program	SHELXL-2018/3 (Sheldrick, 2018)	
Function minimized	$\Sigma\, w(F_o^2 - F_c^2)^2$	
Data / restraints / parameters	5923 / 530 / 435	
Goodness-of-fit on F^2	1.111	
Final R indices	5203 data; I>2σ(I)	R1 = 0.0496, wR2 = 0.1454
	all data	R1 = 0.0564, wR2 = 0.1532
Weighting scheme	$w=1/[\sigma^2(F_o^2)+(0.0900P)^2+12.5856P]$ where $P=(F_o^2+2F_c^2)/3$	
Largest diff. peak and hole	1.180 and -0.780 eÅ^{-3}	
R.M.S. deviation from mean	0.079 eÅ^{-3}	

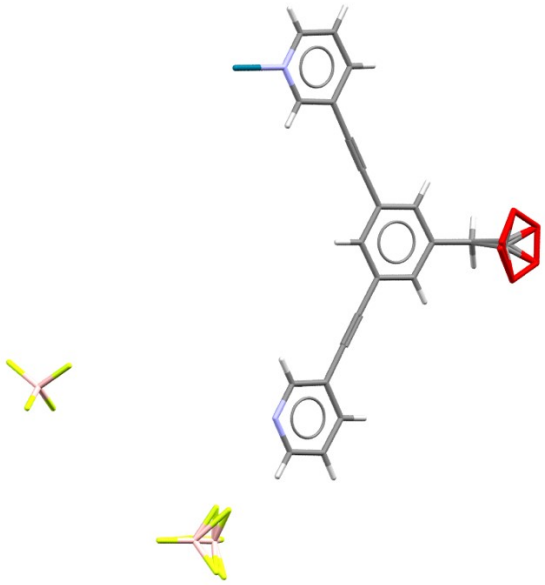

Figure B: Asymmetric unit of $[Pd_2\mathbf{L2}_4]^{4+}$ displayed as capped sticks.

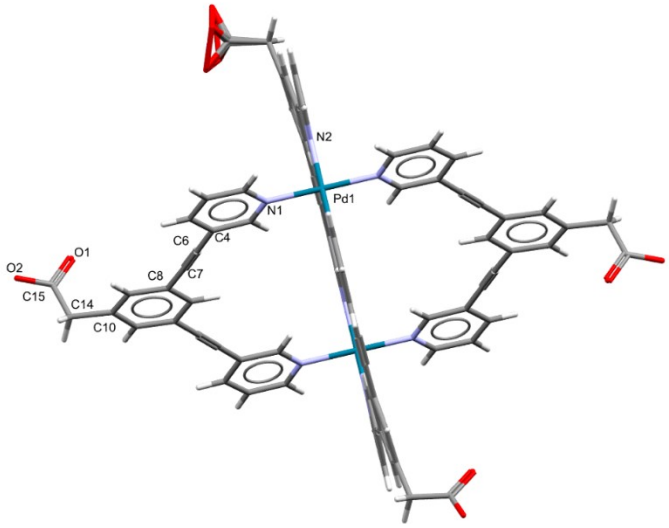

Figure C: Representation of the selected geometric parameters of $[Pd_2\mathbf{L2}_4]^{4+}$. Atoms are displayed as capped sticks.

Table S2: Selected geometric parameters of $[Pd_2\mathbf{L2}_4]^{4+}$ (Å, °).

Pd1–N1	2.027(3)	C10–C14	1.503(5)
Pd1–N2	2.028(3)	C14–C15	1.425(13)
N1–Pd1–N2	89.92(11)	C10–C14–C15	112.0(8)
C4–C6	1.432(4)	C15–O1	1.308(11)
C4–C6–C7	179.5(4)	C15–O2	1.315(14)
C6–C7	1.192(5)	C14–C15–O1	122.9(16)
C7–C8	1.432(4)	C14–C15–O2	117.0(13)
C6–C7–C8	178.7(4)	O1–C15–O2	119.1(15)

Table S3: Symmetry operations of $[Pd_2\mathbf{L2}_4]^{4+}$.

Symm. Op.	Detailed Description	Order	Type
x,y,z	Identity	1	1
-x,y,-z	2-fold rotation axis with direction [0, 1, 0] at 0, y, 0	2	2
-x,-y,-z	Inversion centre at [0, 0, 0]	2	-1
x,-y,z	Mirror plane perpendicular to [0, 1, 0]	2	-2
1/2+x,1/2+y,z	Centring vector [1/2, 1/2, 0]	1	1
1/2-x,1/2+y,-z	2-fold screw axis with direction [0, 1, 0] at 1/4, y, 0 with screw component [0, 1/2, 0]	2	2
1/2-x,1/2-y,-z	Inversion centre at [1/4, 1/4, 0]	2	-1
1/2+x,1/2-y,z	Glide plane perpendicular to [0, 1, 0] with glide component [1/2, 0, 0]	2	-2

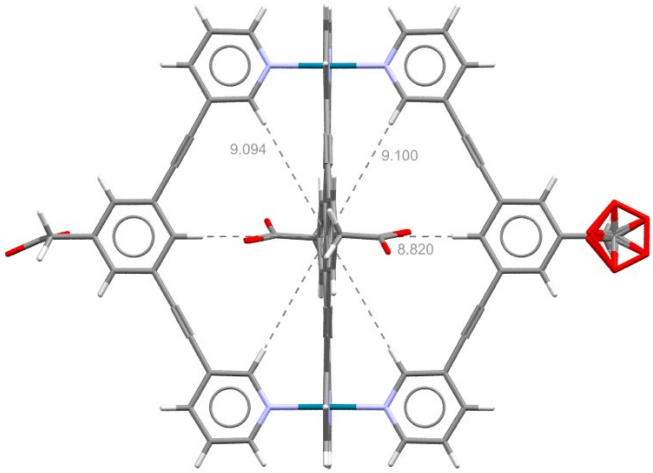

Figure D: Calculation method for the pore size of $[Pd_2\mathbf{L2}_4]^{4+}$. Distances of the innermost hydrogen atoms minus 2x the covalent radius of hydrogen (0.31 Å) leading to an average pore size of 8.38 Å.

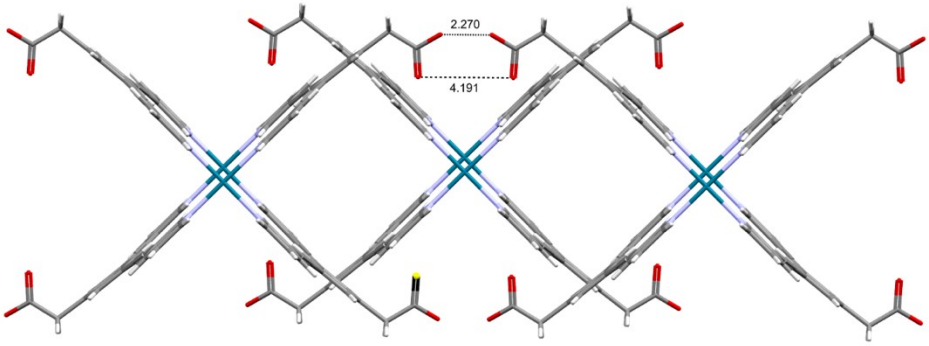

Figure E: Detailed view on the crystal packing along a-axis of $[Pd\mathbf{L2}_4]^{4+}$. Distances of neighbouring $-COO^-$ groups along leading to linear packing by presumably hydrogen bonding with 2.270 and 4.1191 Å.

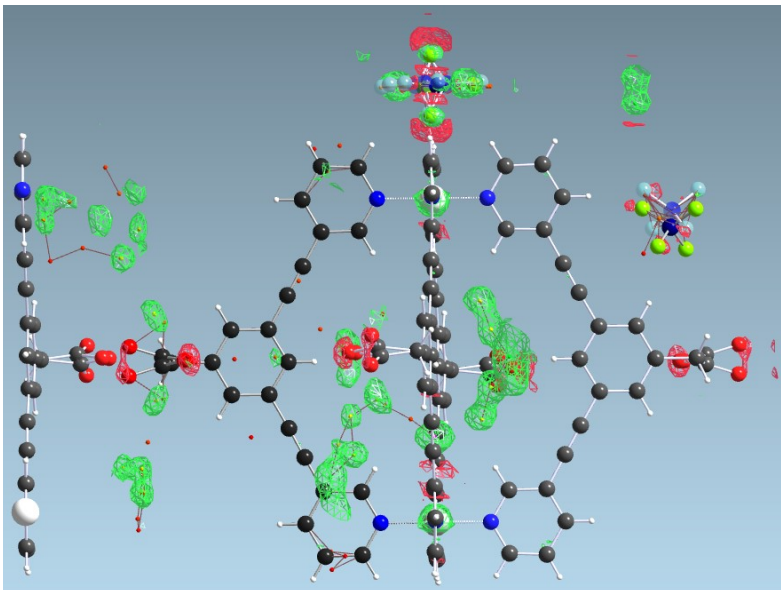

Figure F: Depiction of the residual electron density before application of PLATON/SQUEEZE procedure for solvent masking (visualized in SHELXLE). Visual inspection of the residual electron density showed no obvious tetrahedral geometry as it would be expected for BF_4^- anion, however, linearly chain-like arranged electron density, presumably corresponding to disordered diethyl ether solvent molecules can be found. A void volume of 2514 $Å^3$ and an electron counts of 761 e^- in the unit cell was determined, corresponding to roughly 16 diethylether molecules per unit cell (i.e. 4 per cage).

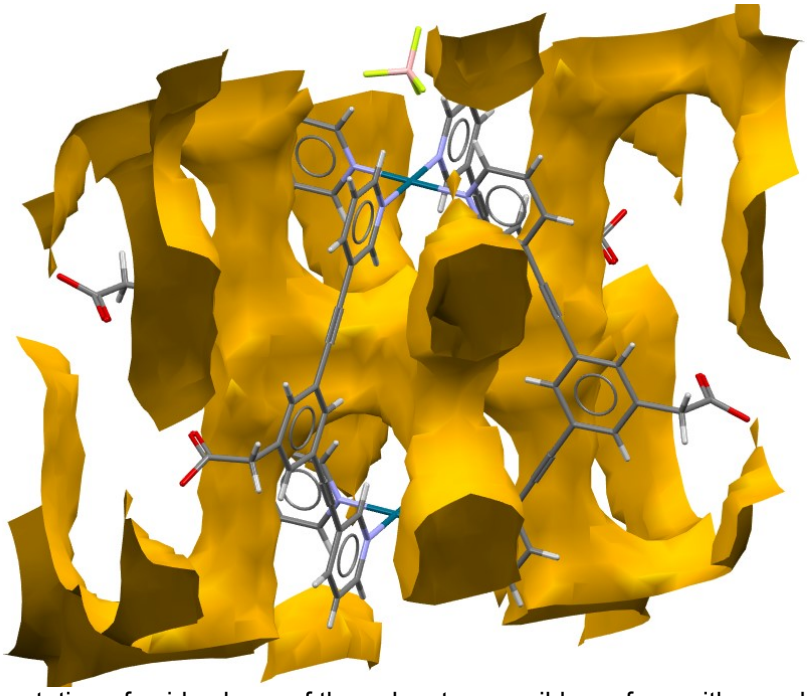

Figure G: Representation of void volume of the solvent accessible surface with a probe radius of 1.2 Å displayed in Mercury after PLATON/SQUEEZE procedure.